# Supporting Information

## Versatile Nature of Anthanthrone Based Polymers as Active Multifunctional Semiconductors for Various Organic Electronic Devices

Qian Liu,[a] Yang Wang,[b] Lingeswaran Arunagiri,[c] Muhammad Khatib,[d] Sergei Manzhos,[e] Krishna Feron,[fg] Steven E. Bottle,[ah] Hossam Haick,[d] He Yan,[c] Tsuyoshi Michinobu[b] and Prashant Sonar*[ah]

[a.] *School of Chemistry and Physics, Science and Engineering Faculty, Queensland University of Technology, Brisbane, QLD 4000, Australia.*
[b.] *Department of Materials Science and Engineering, Tokyo Institute of Technology, 2-12-1 Ookayama, Meguro-ku, Tokyo 152-8552, Japan.*
[c.] *Department of Chemistry and Hong Kong Branch of Chinese National Engineering Research Centre for Tissue Restoration and Reconstruction, Hong Kong University of Science and Technology, Clear Water Bay, Kowloon, Hong Kong, China.*
[d.] *Department of Chemical Engineering and Russell Berrie Nanotechnology Institute Technion - Israel Institute of Technology, Haifa 3200003, Israel.*
[e.] *Centre Énergie Matériaux Télécommunications, Institut National de la Recherche Scientifique, 1650 boulevard Lionel-Boulet, Varennes, QC J3X1S2, Canada.*
[f.] *CSIRO Energy Centre, 10 Murray Dwyer Circuit, Mayfield West, NSW 2304, Australia.*
[g.] *Centre for Organic Electronics, University of Newcastle, Callaghan, NSW 2308, Australia.*
[h.] *Centre for Materials Science, Queensland University of Technology, Brisbane, QLD 4000, Australia.*

## Experimental Section

### General Measurements

All the reagents and chemicals were purchased from commercially available suppliers such as Sigma-Aldrich, Bide Pharmatech and TCI. The chemicals were used as received without further purification unless otherwise noted. All the reactions were carried out under argon atmosphere. The NMR spectra were recorded on a Bruker 600 spectrometer, using the residual solvent resonance of $CDCl_3$, and the chemical shifts are given in ppm. Gel permeation chromatography (GPC) was measured by a JASCO GULLIVER 1500 equipped with a pump (PU-2080 Plus), an absorbance detector (RI-2031 Plus), and two Shodex GPC KF-803 columns (8.0 mm I.D. × 300 mm L) based on a conventional calibration curve using polystyrene standards. *o*-Dichlorobenzene (40°C) was used as the carrier solvent at the flow rate of 0.5 mL/min. The molecular weights were calculated based on a conventional calibration curve using polystyrene standards. Thermal stability of polymers was measured using a Pegasus Q500 TGA thermogravimetric analyser under nitrogen atmosphere at a heating rate of 10°C/min from 20°C to 800°C. Differential scanning calorimetry (DSC) measurements were conducted under nitrogen atmosphere using a Chimaera instrument Q100 DSC at a heating rate of 10°C/min and cooling rate of 5°C/min between 20 and 300°C. Absorption spectra were recorded on a Carry 50 UV-

Vis spectrophotometer. Photoelectron spectroscopy in air (PESA) measurements were conducted using on an AC-2 photoelectron spectrometer (Riken-Keiki Co.). Density Functional Theory (DFT)[1] calculations were performed in Gaussian 16[2] using the B3LYP[3] functional and the Lanl2dz basis set. PCM (polarizable continuum) model[4] of the chloroform solvent was used. Optical properties were computed with Time-Dependent DFT[5] using 10 lowest singlet excited states. The alkyl chains were abridged in the DFT model to moderate the cpu cost as they do not perceptibly affect electronic properties of the oligomers.

**Fabrication and Characterization of Organic Field-Effect Transistors**

Top-contact/bottom-gate (TC/BG) organic field-effect transistors were fabricated on $n^{++}$-Si/$SiO_2$ substrates in which $n^{++}$-Si and $SiO_2$ were used as the gate electrode and gate dielectric, respectively. The substrates were subjected to cleaning and modified with octadecyltrimethoxysilane (OTMS) to form a self-assembled monolayer (SAM). Thin films of the polymers were deposited on the treated substrate by spin-coating the polymer solutions inside an argon-filled glovebox followed by thermal annealing. The details of the thermal annealing conditions were 200, 250 or 270°C for 10 min in an argon-filled glovebox. After the polymer thin film deposition, ~50 nm thick gold was deposited as the source and drain contacts using a shadow mask. The devices had a channel length (L) of 100 μm and a channel width (W) of 1 mm. The field-effect transistor performance was measured under laboratory ambient conditions using a Keithley 4200 parameter analyzer on a probe stage. The carrier mobilities, μ, were calculated from the data in the saturated regime according to the following equation:

$I_{SD} = (W/2L)C_i\mu(V_{GS} - V_{th})^2$

where $I_{SD}$ is the drain current in the saturated regime, W and L are the semiconductor channel width and length, respectively, $C_i$ ($C_i$ = 13.7 nF $cm^{-2}$) is the capacitance per unit area of the gate dielectric layer, and $V_{GS}$ and $V_{th}$ are the gate voltage and threshold voltage, respectively. $V_{GS}-V_{th}$ of the devices was determined from the square root values of $I_{SD}$ at the saturated regime.

**Atomic Force Microscopy (AFM) Measurements**

The AFM samples were prepared by spin-coating the polymer solutions on a Si/$SiO_2$ substrate. Both the pristine and thermally treated films were analysed by a Seiko Instruments SPA-400 with a Seiko Instruments DF-20 stiff cantilever.

**Fabrication of the OFET Sensor**

OFETs were prepared on silicon wafers capped with 300 nm thermal oxide. A Ti/Au (10/200 nm) bottom-gate electrode was deposited by electron beam evaporation. A total of 49 pairs of circular interdigitated source and drain Au (300 nm) electrodes were prepared using photolithography and electron-beam evaporation. The outer diameter of the circular electrode area was 3 mm. The gap between the 2 adjacent electrodes (channel length) and the width of each electrode were 25 and 5 μm, respectively. Silicon wafers were treated with octadecyltrichlorosilane (ODTS)/toluene solution ($60 \times 10^{-3}$ M, 20 mL) for 10 h. Finally, organic semiconductors (2 mg/mL in chloroform/dichlorobenzene) were deposited on the OTS-treated substrates by drop-casting.

**OFET-Sensor Measurements**

The OFET-based sensor was loaded into a stainless-steel chamber of ~300 $cm^3$. For the exposure of pure volatile organic compounds (VOCs), a computer-controlled bubbler was filled with the corresponding liquid, and then $N_2$ was bubbled through. The resulting gas mixture ($N_2$ and organic vapour) was diluted to obtain the desired concentrations. Vacuum was used as a baseline between exposure cycles. Source-drain current $I_{SD}$ versus gate voltage $V_G$ measurements (swept between 10 and -60 V with -1 V steps and -60 V constant source-drain voltage, $V_{SD}$) were carried out using a Keithley 2636A system SourceMeter and a 3706 system Switch/Multimeter.

**Discriminant Function Analysis (DFA)**

DFA analysis was done using JMP 15 software. DFA finds linear combinations of sensing features that separate two or more classes of objects. For the discrimination between all four VOCs, CV1 and CV2, a linear combination of the responses ($X_i = \Delta I_{on}/|I_{on}|$) of the four polymers, were used. $CV1 = 0.091 \times X_{PANT} + 0.309 \times X_{TBO} - 0.326 \times X_{TBT} + 0.464 \times X_{TffBT} + 0.423$, and $CV2 = 0.043 \times X_{PANT} + 1.143 \times X_{TBO} - 0.006 \times X_{TBT} - 0.764 \times X_{TffBT} + 0.150$. Responses were calculated from 3 repetitions of exposure to 4 VOC concentrations (160, 320, 640, 1280 ppm)

**OPV Device Fabrication**

For all the OPV devices, prepatterned ITO-coated glass substrates (sheet resistance of 15 Ω/sq) were cleaned using ultrasonic cleaner in detergent, deionized water, acetone, and isopropanol successively for 30 mins each step. UV-ozone treatment using Novascan PSD series digital ultraviolet ozone system was performed for 30 mins before the ITO substrates were transferred to a dry air-filled glovebox to spin coat PEDOT:PSS at 5000rpm for 30 s and then annealed at 150°C for 12 mins. For active layer solution preparation, donor polymer:acceptor was dissolved in CB and 0.5% 1, 8-diiodooctane (DIO) with the weight ratio of 1:1.5 (donor concentration of 12-14 mg/ml) and stirred at 100°C for 2 hrs before spin coating at 2500 rpm for 1 min. The active layer film was then annealed at 100 °C for 10 mins. PFN-Br was dissolved in methanol at the concentration of 0.5 mg/ml and spin coated at 2000 rpm for 30 s on the active layer film. Later, Ag (~250 nm) was thermally evaporated at a vacuum level of $\leq 1.5 \times 10^{-4}$ Pa at rates between 2-5 Å/s. After electrode deposition, the devices were encapsulated using EPO-TEK (OG154-1) epoxy in a nitrogen-filled glove box and transferred to ambient conditions to further conduct *J*–*V* measurements using a Keithley 2400 source meter unit under AM 1.5G (100 $mW/cm^2$) by a Newport solar simulator. The light intensity was calibrated using a standard Si diode (with KG5 filter, purchased from PV Measurement) to bring spectral mismatch to unity. Typical cells have a device area of 5.9 $mm^2$ defined by a metal mask with an aperture aligned with the device area. The photovoltaic performance of the devices was not confirmed from independent certification laboratories. External quantum efficiency (EQE) spectra were measured using an EQE (Enlitech QS) system equipped with a standard Si diode with the monochromatic light generated from a Newport 300 W lamp source.

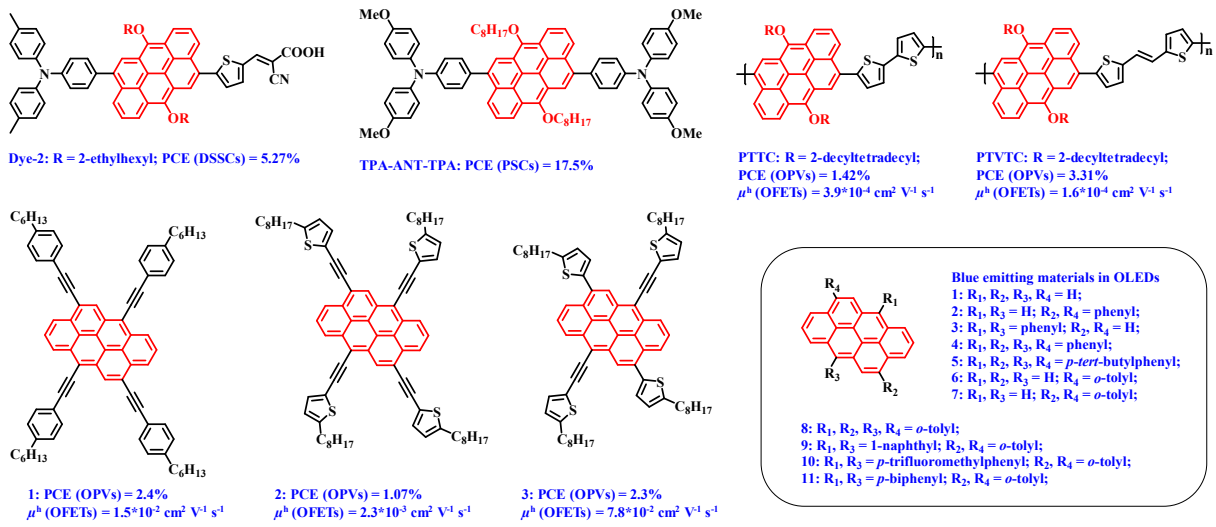


**Scheme S1.** Reported ANT materials used in electronic devices in literature. DSSCs: Dye-Sensitised Solar Cells; PSCs: Perovskite Solar Cells; OPVs: Organic Photovoltaics; OFETs: Organic Field-Effect Transistors; OLEDs: Organic Light Emitting Diodes.[6-11]

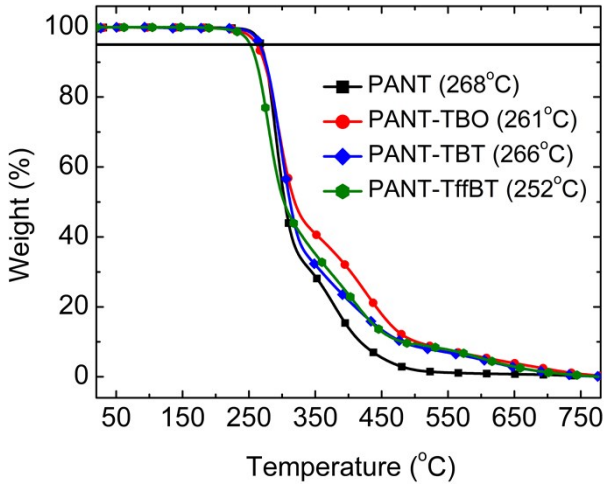


**Figure S1.** The TGA thermograms of four polymers measured under argon atmosphere with a heating rate of 10 °C/min from room temperature to 800 °C.

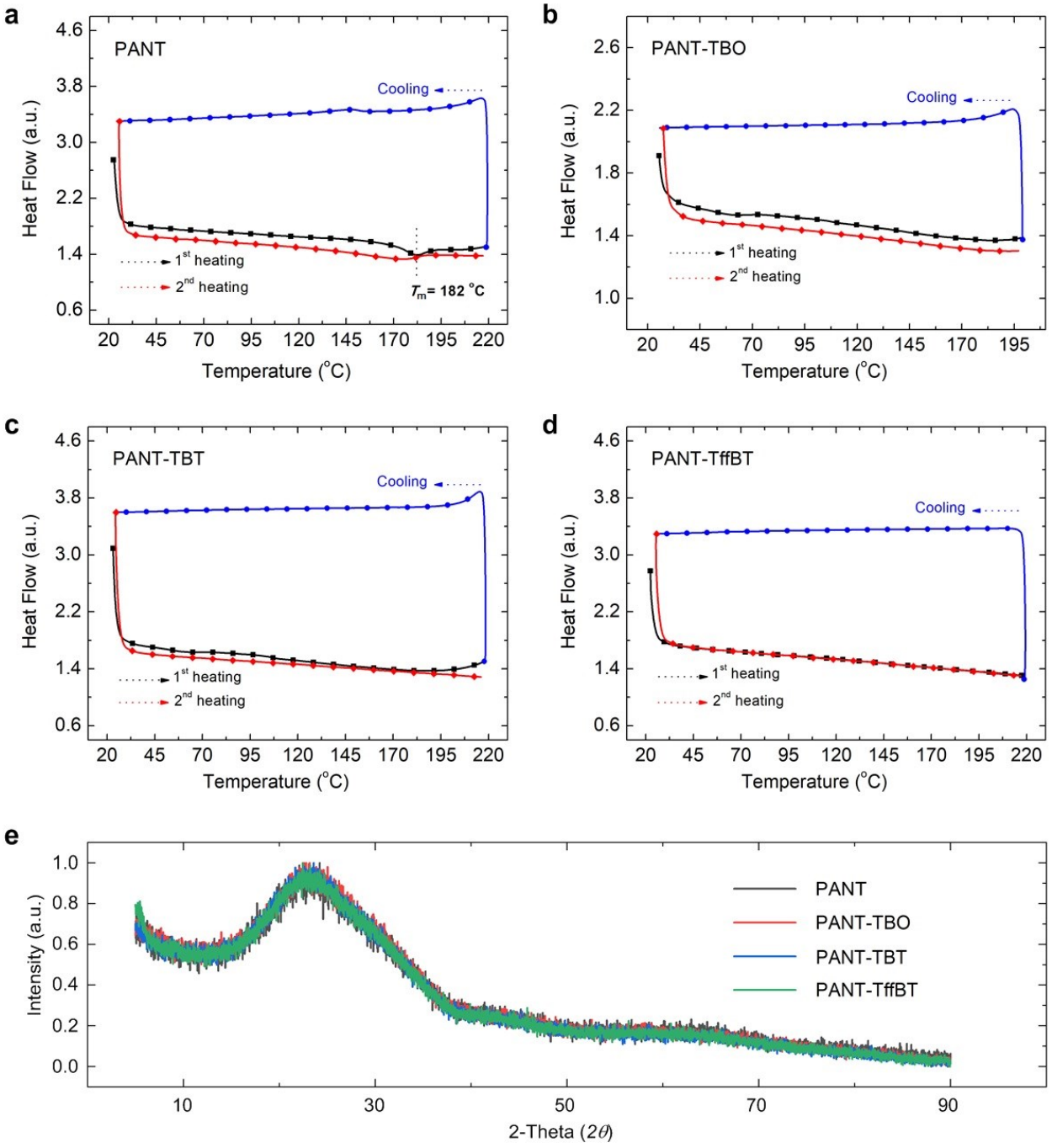


**Figure S2.** (a-d) The DSC thermograms of four polymers measured under argon atmosphere with a heating/cooling rate of 10/5 °C/min. (e) The thin film X-ray diffraction spectra. No obvious crystalline peaks are observed for all four polymers, indicating that the overall crystallinity of four polymers are low.

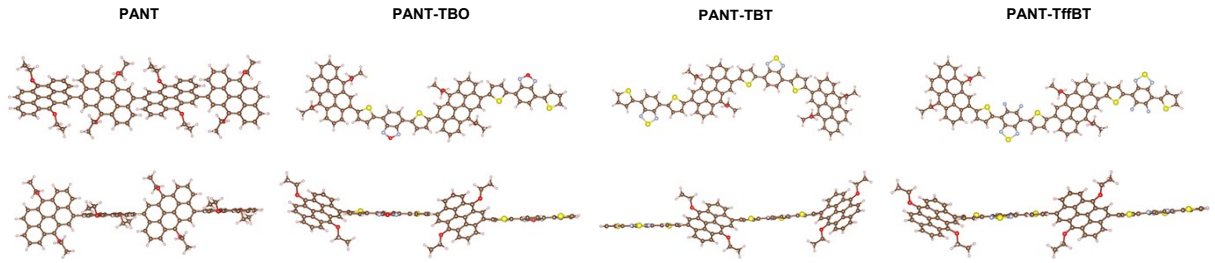


**Figure S3.** DFT calculated structures of dimers: front (upper) and side (down) views.

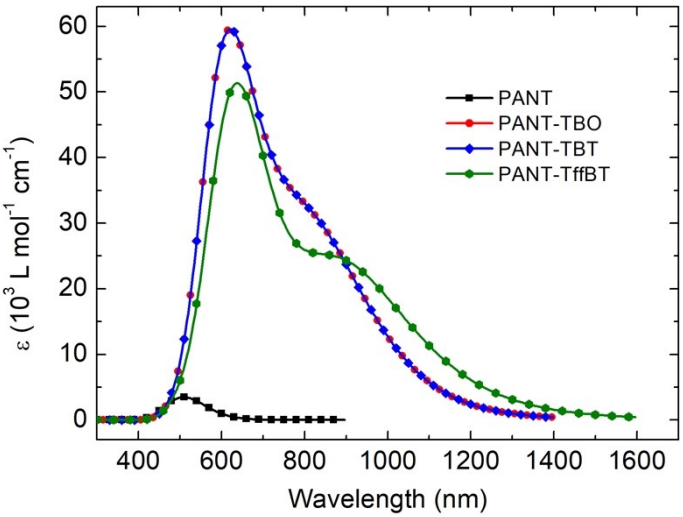


**Figure S4.** DFT calculated absorption spectra of the dimer models. PANT exhibited a clear low absorption coefficient, which is consistent with the experimental results. That is resulted from the weak intramolecular charge transfer (ICT) between donor and donor than that of between donor and acceptor for other three donor-acceptor polymers.

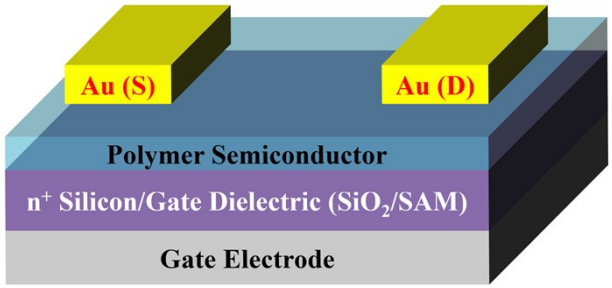


**Figure S5.** The OFET structure used in this study. Device configuration: bottom gate top contact (BG/TC).

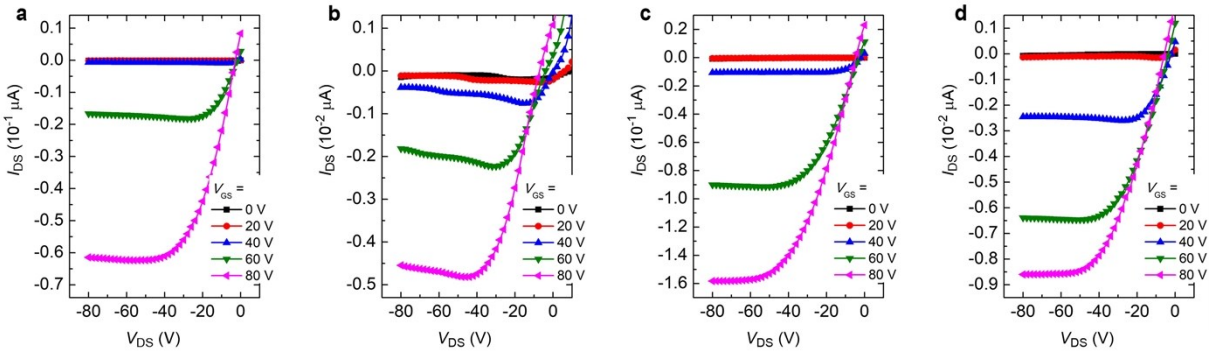


**Figure S6.** The output curves of OFETs based on the four polymers: (a) PANT, (b) PANT-TBO, (c) PANT-TBT, (d) PANT-TffBT.

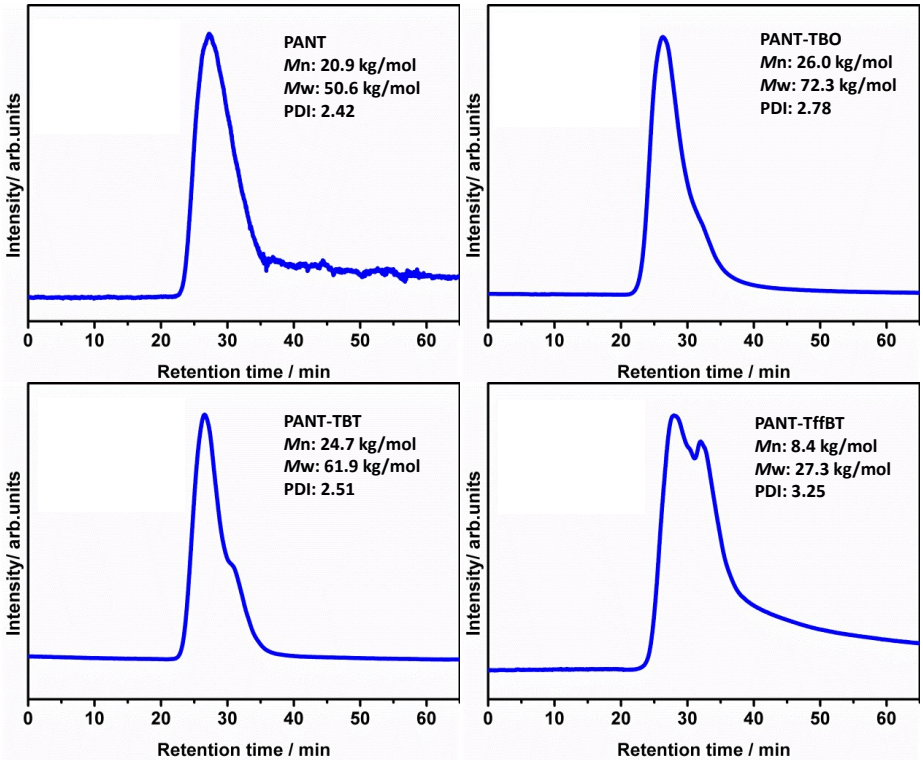


**Figure S7.** Molecular weight measurements of the polymers using gel permeation chromatography (GPC). (Eluent: *o*-dichlorobenzene at 40 °C) Note: the low molecular weight of PANT-TffBT could be resulted from the low solubility. When purifying this polymer by using Soxhlet extraction, the polymer is extracted with chlorobenzene at high temperature, while the reaction is conducted at 80°C. That means the reaction might terminate earlier than other three polymers because of low solubility, resulting in lower molecular weight.

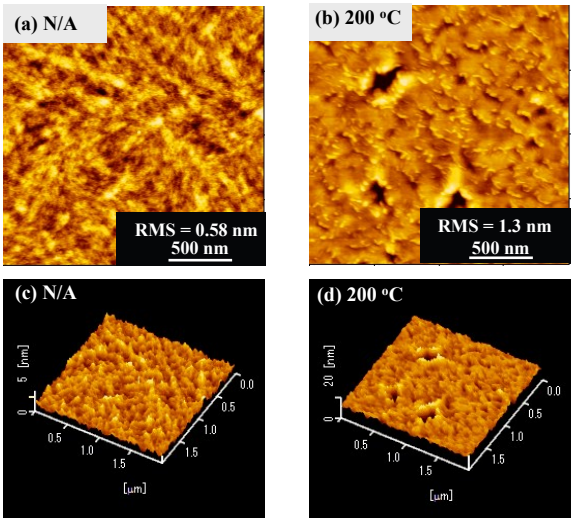


**Figure S8.** Tapping-mode AFM topography images of the PANT thin films (a) without annealing; (b) annealing at 200 °C for 10 min and their corresponding 3D profiles (c) without annealing; (d) annealing at 200 °C.

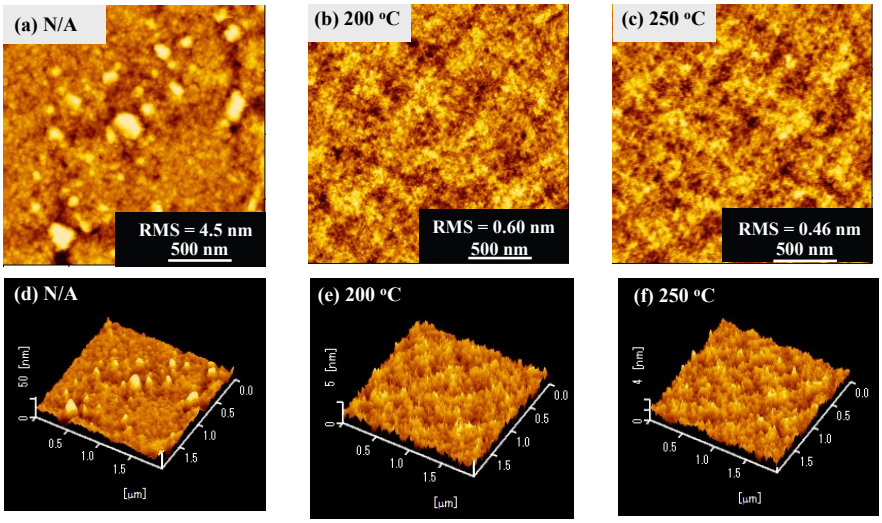


**Figure S9.** Tapping-mode AFM topography images of the PANT-TBO thin films (a) without annealing; (b) annealing at 200 °C; (c) annealing at 250 °C for 10 min and their corresponding 3D profiles (d) without annealing; (e) annealing at 200 °C; (f) annealing at 250 °C.

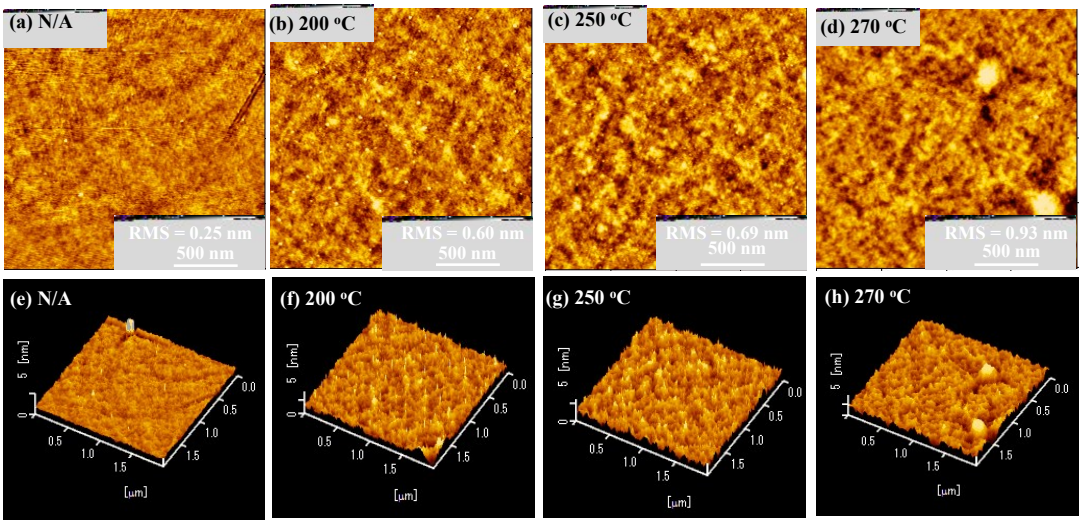


**Figure S10.** Tapping-mode AFM topography images of the PANT-TBT thin films (a) without annealing; (b) annealing at 200 °C; (c) annealing at 250 °C; (d) annealing at 270 °C for 10 min and their corresponding 3D profiles (e) without annealing; (f) annealing at 200 °C; (g) annealing at 250 °C; (h) annealing at 270 °C.

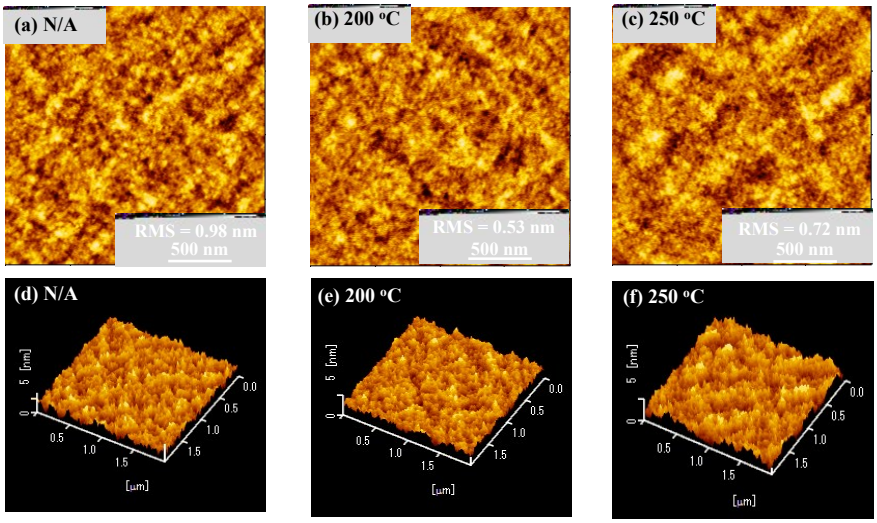


**Figure S11.** Tapping-mode AFM topography images of the PANT-TffBT thin films (a) without annealing; (b) annealing at 200 °C; (c) annealing at 250 °C for 10 min and their corresponding 3D profiles (d) without annealing; (e) annealing at 200 °C; (f) annealing at 250 °C.

**Table S1.** Summary of OFETs performance based on PANT.

| Annealing Temp. | $\mu_{h\ max.}$ ($cm^2\ V^{-1}\ s^{-1}$) [a] | $\mu_{h\ avg.}$ ($cm^2\ V^{-1}\ s^{-1}$) [b] | $V_{th}$ (V) | $I_{ON}/I_{OFF}$ |
|---|---|---|---|---|
| N/A | $1.5\times10^{-3}$ | $1.3\times10^{-3}$ | -38 | $10^2$-$10^3$ |
| 200 °C | **$2.2\times10^{-3}$** | $2.0\times10^{-3}$ | -32 | $10^3$-$10^4$ |
| 250 °C [c] | NA | NA | NA | NA |

[a] The mobility values under optimized annealing conditions are indicated in boldface. [b] The average values are calculated from 3 devices. [c] The polymer thin film seems to experience unfavorable unknow change after thermal annealing at 250 °C because of the observation of color change from yellow to dark.

**Table S2.** Summary of OFETs performance based on PANT-TBO.

| Annealing Temp. | $\mu_{h\ max.}$ ($cm^2\ V^{-1}\ s^{-1}$) [a] | $\mu_{h\ avg.}$ ($cm^2\ V^{-1}\ s^{-1}$) [b] | $V_{th}$ (V) | $I_{ON}/I_{OFF}$ |
|---|---|---|---|---|
| N/A | $1.2\times10^{-4}$ | $1.1\times10^{-4}$ | -46 | $10^2$-$10^3$ |
| 200 °C | **$2.9\times10^{-4}$** | $2.3\times10^{-4}$ | -33 | $10^3$-$10^4$ |
| 250 °C | $2.1\times10^{-4}$ | $1.5\times10^{-4}$ | -50 | $10^3$-$10^4$ |

[a] The mobility values under optimized annealing conditions are indicated in boldface. [b] The average values are calculated from 3 devices.

**Table S3.** Summary of OFETs performance based on PANT-TBT.

| Annealing Temp. | $\mu_{h\ max.}$ ($cm^2\ V^{-1}\ s^{-1}$) [a] | $\mu_{h\ avg.}$ ($cm^2\ V^{-1}\ s^{-1}$) [b] | $V_{th}$ (V) | $I_{ON}/I_{OFF}$ |
|---|---|---|---|---|
| N/A | $1.1\times10^{-3}$ | $9.3\times10^{-4}$ | -12 | $10^2$-$10^3$ |
| 200 °C | $1.7\times10^{-3}$ | $1.6\times10^{-3}$ | -10 | $10^3$-$10^4$ |
| 250 °C | **$4.5\times10^{-3}$** | $3.6\times10^{-3}$ | -16 | $10^3$-$10^4$ |
| 270 °C [c] | $2.5\times10^{-3}$ | $1.9\times10^{-3}$ | -15 | $10^3$-$10^4$ |

[a] The mobility values under optimized annealing conditions are indicated in boldface. [b] The average values are calculated from 3 devices. [c] The hole mobility at 270°C might be the performance of OFETs with TBT-based materials as the channel semiconductor. From the TGA thermograms, PANT-TBT should have decomposed at 270°C, however TBT and benzene-based materials were reported to have a decomposition temperature of around 400°C.[12]

**Table S4.** Summary of OFETs performance based on PANT-TffBT.

| Annealing Temp. | $\mu_{h\ max.}$ ($cm^2\ V^{-1}\ s^{-1}$) [a] | $\mu_{h\ avg.}$ ($cm^2\ V^{-1}\ s^{-1}$) [b] | $V_{th}$ (V) | $I_{ON}/I_{OFF}$ |
|---|---|---|---|---|
| N/A | $1.1\times10^{-4}$ | $1.1\times10^{-4}$ | -50 | $10^2$-$10^3$ |
| 200 °C | **$5.0\times10^{-4}$** | $4.5\times10^{-4}$ | -60 | $10^3$-$10^4$ |
| 250 °C | $3.7\times10^{-4}$ | $2.3\times10^{-4}$ | -60 | $10^3$-$10^4$ |

[a] The mobility values under optimized annealing conditions are indicated in boldface. [b] The average values are calculated from 3 devices.

**Table S5.** Summary of OFETs performance based on reported ANT-based materials.

| Material [a] | Condition | $\mu_{h\ max.}$ ($cm^2\ V^{-1}\ s^{-1}$) | $\mu_{h\ avg.}$ ($cm^2\ V^{-1}\ s^{-1}$) | $V_{th}$ (V) | $I_{ON}/I_{OFF}$ |
|---|---|---|---|---|---|
| Comp. 1 [b] | As cast | $5.2\times10^{-4}$ | $4.3\times10^{-4}$ | 5 | $10^4$ |
| | Toluene annealing | $1.0\times10^{-2}$ | $8.9\times10^{-3}$ | 4 | $10^5$ |
| | Cyclohexane annealing | $1.5\times10^{-2}$ | $1.3\times10^{-2}$ | 3 | $10^5$ |
| Comp. 2 [b] | As cast | $1.5\times10^{-4}$ | $1.0\times10^{-4}$ | 9 | --- |
| | Toluene annealing | $2.3\times10^{-3}$ | $2.0\times10^{-3}$ | 19 | $10^3$ |
| | Cyclohexane annealing | $1.7\times10^{-3}$ | $1.4\times10^{-3}$ | 19 | $10^3$ |
| Comp. 3 [b] | As cast | $6.7\times10^{-3}$ | $6.4\times10^{-3}$ | -9 | $10^5$ |
| | Toluene annealing | $7.8\times10^{-2}$ | $6.5\times10^{-2}$ | -6 | $10^6$ |
| | Cyclohexane annealing | $4.9\times10^{-2}$ | $3.4\times10^{-2}$ | -6 | $10^6$ |
| PTTC | As cast | $3.9\times10^{-4}$ | --- | -7.8 | $4\times10^4$ |
| PTVTC | As cast | $1.6\times10^{-4}$ | --- | -7.4 | $3\times10^4$ |

[a] The structures of materials and the data source are shown in **Scheme S1**. [b] The average values are calculated from 4 devices. Note: thermal annealing treatment didn't improve the OFET device performances for compounds 1-3.

**Table S6.** Summary of the sensitivity and limit of detection (LOD) toward different gases.

| | | Acetic acid | Octane | Toluene | Propanol |
|---|---|---|---|---|---|
| LOD [ppm] | PANT | 2.8 | --- | 260 | 188 |
| | PANT-TBO | 270 | 590 | --- | 110 |
| | PANT-TBT | 4/35* | 240 | 70 | 175 |
| | PANT-TffBT | 140 | 610 | 240 | 210 |
| Sensitivity [$10^3\times ppm^{-1}$] | PANT | -31.0±5.1 | --- | -2.9±1.3 | -1.6±0.7 |
| | PANT-TBO | -31.0±2.1 | -2.5±0.4 | --- | -1.6±0.3 |
| | PANT-TBT | 161±7/-37±2* | 65.2±3.4 | -3.5±1.1 | -2.1±0.2 |
| | PANT-TffBT | -17±0.8 | -0.9±0.2 | -2.2±0.4 | -1.7±0.3 |

* Two different sensing mechanisms are involved where each one starts at a different concentration. (---) No detection in the tested range of concentrations.

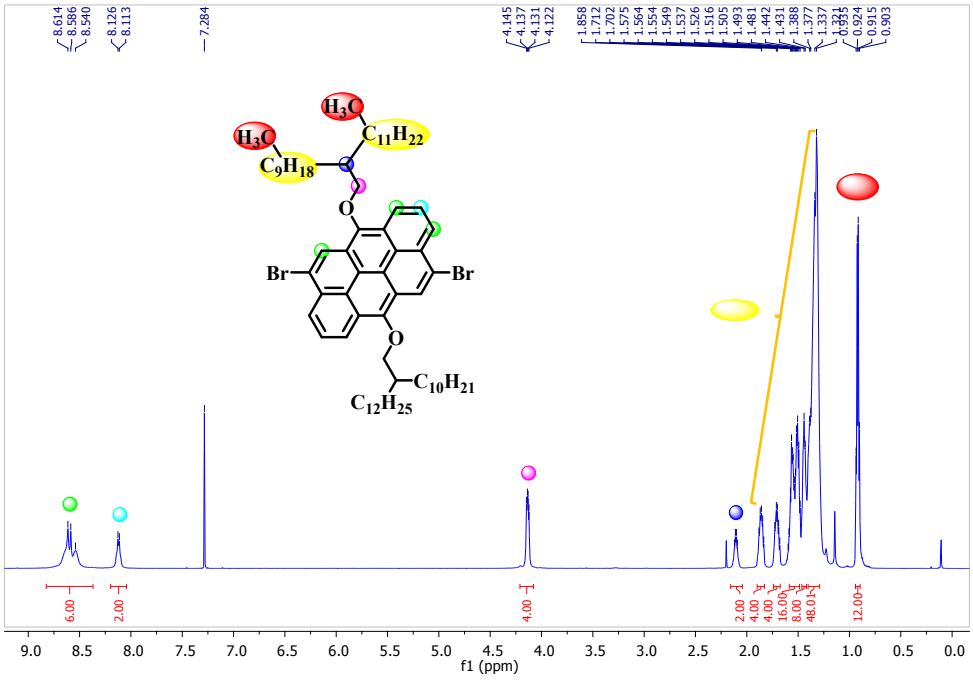


**Figure S12.** $^{1}$H NMR spectrum of C24-ANT in $CDCl_3$.

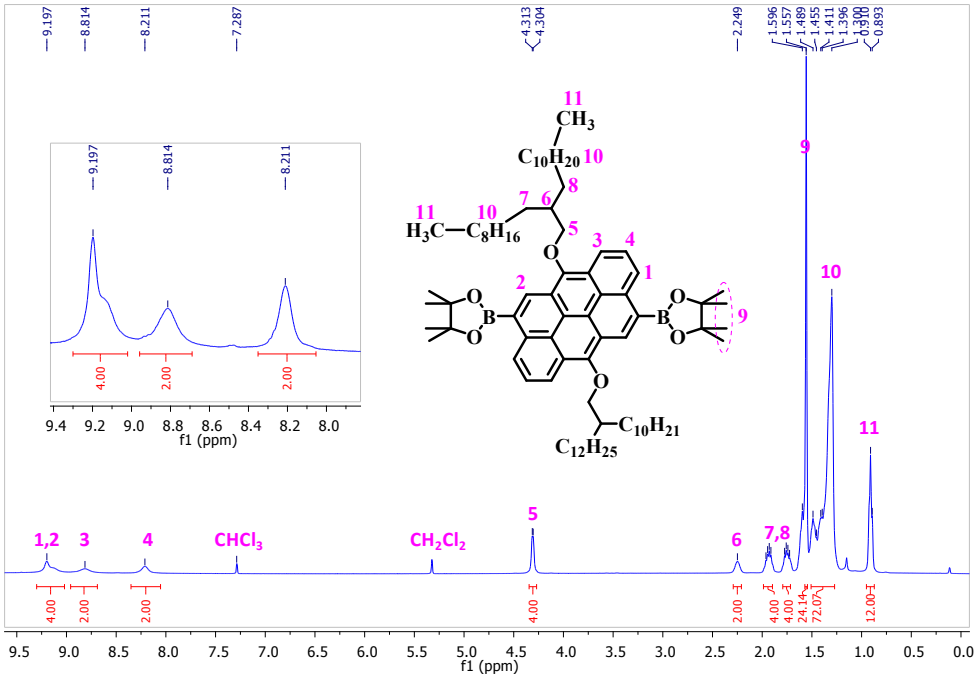


**Figure S13.** $^{1}$H NMR spectrum of BE-C24-ANT in $CDCl_3$.

## References


1. W. Kohn and L. J. Sham, *Phys. Rev.*, 1965, **140**, A1133.
2. M. Frisch, G. Trucks, H. Schlegel, G. Scuseria, M. Robb, J. Cheeseman, G. Scalmani, V. Barone, B. Mennucci and G. Petersson, 2005.
3. A. D. Becke, *J. Chem. Phys.*, 1993, **98**, 5648-5652.
4. G. Scalmani and M. J. Frisch, *J. Chem. Phys.*, 2010, **132**, 114110.
5. C. Adamo and D. Jacquemin, *Chem. Soc. Rev.*, 2013, **42**, 845-856.
6. Y. J. Kim, J. S. Lee, J. Hong, Y. Kim, S. B. Lee, S.-K. Kwon, Y.-H. Kim and C. E. Park, *J. Polym. Sci., Part A: Polym. Chem.*, 2016, **54**, 2559-2570.
7. J. Hong, Y. J. Kim, Y.-H. Kim and C. E. Park, *Macromol. Chem. Phys.*, 2016, **217**, 2116-2124.
8. J.-B. Giguère, N. S. Sariciftci and J.-F. Morin, *J. Mater. Chem. C*, 2015, **3**, 601-606.
9. H. D. Pham, T. T. Do, J. Kim, C. Charbonneau, S. Manzhos, K. Feron, W. C. Tsoi, J. R. Durrant, S. M. Jain and P. Sonar, *Adv. Energy Mater.*, 2018, **8**, 1703007.
10. Y. Geng, C. Yi, M. P. Bircher, S. Decurtins, M. Cascella, M. Grätzel and S.-X. Liu, *RSC Adv.*, 2015, **5**, 98643-98652.
11. B. K. Shah, D. C. Neckers, J. Shi, E. W. Forsythe and D. Morton, *Chem. Mater.*, 2006, **18**, 603-608.
12. Y. Li, J. Wang, Y. Liu, M. Qiu, S. Wen, X. Bao, N. Wang, M. Sun and R. Yang, *ACS Appl. Mater. Interfaces*, 2016, **8**, 26152-26161.